



**HAL**  
open science

## Investigating $\delta^{13}\text{C}$ values in stalagmites from tropical South America for the last two millennia

Valdir Felipe Novello, Francisco William da Cruz, Mathias Vuille, José Leandro Pereira Silveira Campos, Nicolás Misailidis Stríkis, James Apaéstegui, Jean-Sébastien Moquet, Vitor Azevedo, Angela Ampuero, Giselle Utida, et al.

### ► To cite this version:

Valdir Felipe Novello, Francisco William da Cruz, Mathias Vuille, José Leandro Pereira Silveira Campos, Nicolás Misailidis Stríkis, et al.. Investigating  $\delta^{13}\text{C}$  values in stalagmites from tropical South America for the last two millennia. *Quaternary Science Reviews*, 2021, 255, pp.106822. <10.1016/j.quascirev.2021.106822>. <insu-03141092>

**HAL Id: insu-03141092**

**<https://insu.hal.science/insu-03141092v1>**

Submitted on 28 Jan 2025

HAL is a multi-disciplinary open access archive for the deposit and dissemination of scientific research documents, whether they are published or not. The documents may come from teaching and research institutions in France or abroad, or from public or private research centers.

L'archive ouverte pluridisciplinaire HAL, est destinée au dépôt et à la diffusion de documents scientifiques de niveau recherche, publiés ou non, émanant des établissements d'enseignement et de recherche français ou étrangers, des laboratoires publics ou privés.



Distributed under a Creative Commons CC BY 4.0 - Attribution - International License

# 1 Investigating $\delta^{13}\text{C}$ values in stalagmites from tropical 2 South America for the last two millennia

3 Valdir Felipe Novello<sup>a\*</sup>; Francisco William da Cruz<sup>a</sup>, Mathias Vuille<sup>b</sup>, José Leandro  
4 Pereira Silveira Campos<sup>a</sup>, Nicolás Misailidis Stríkis<sup>c</sup>, James Apaéstegui<sup>d</sup>, Jean Sebastien  
5 Moquet<sup>e</sup>, Vitor Azevedo<sup>a</sup>, Angela Ampuero<sup>a</sup>, Giselle Utida<sup>a</sup>, Xianfeng Wang<sup>f</sup>, Gustavo  
6 Macedo Paula-Santos<sup>g</sup>, Plinio Jaqueto<sup>h</sup>, Luiz Carlos Ruiz Pessenda<sup>i</sup>, Daniel O Brecker<sup>j</sup>,  
7 Ivo Karmann<sup>a</sup>

8 <sup>a</sup>Institute of Geosciences, University of São Paulo, São Paulo, 05508-080, Brazil.

9 <sup>b</sup>Department of Atmospheric and Environmental Sciences, University at Albany, Albany, 12222, USA.

10 <sup>c</sup>Departamento de Geoquímica, Universidade Federal Fluminense, Niterói, 24020-141, Brazil.

11 <sup>d</sup>Instituto Geofísico del Perú, Lima, 15012, Peru.

12 <sup>e</sup>Institut des Sciences de la Terre d'Orléans, Orléans, 45100, France.

13 <sup>f</sup>Earth Observatory of Singapore, Nanyang Technological University, Jurong West, 639798, Singapore.

14 <sup>g</sup>Institute of Geoscience University of Campinas, 13083-855.

15 <sup>h</sup>Instituto de Astronomia, Geofísica e Ciências Atmosféricas, University of São Paulo, São Paulo, 05508-  
16 090, Brazil

17 <sup>i</sup>Center for Nuclear Energy in Agriculture (CENA), University of São Paulo, São Paulo, 13416-000,  
18 Brazil.

19 <sup>j</sup>Jackson School of Geosciences, University of Texas, Austin, 2305, USA.

20 \*Correspondence to: Valdir F. Novello ([vfnovello@gmail.com](mailto:vfnovello@gmail.com)).

21

## 22 Abstract

23 Due to the many factors controlling  $\delta^{13}\text{C}$  values in stalagmites, complicating their paleoclimatic  
24 and paleoenvironmental interpretation, most studies do not present  $\delta^{13}\text{C}$  values, but instead focus mainly  
25 on  $\delta^{18}\text{O}$  values. This is also the case for most cave studies from tropical South America, where many new  
26  $\delta^{18}\text{O}$  stalagmite records covering the last millennia were recently published. Here, we review the  $\delta^{13}\text{C}$   
27 values in stalagmites, investigating the influence of local hydroclimate, altitude, temperature and  
28 vegetation types on  $\delta^{13}\text{C}$  values in stalagmites, by employing a new dataset composed of published and  
29 unpublished carbon isotope records from various sites in tropical South America. The main factors  
30 influencing  $\delta^{13}\text{C}$  values are associated with the local hydroclimate, followed by minor effects from  
31 temperature. Most of the isotopic records show a significant correlation between the  $\delta^{13}\text{C}$  and  $\delta^{18}\text{O}$  values,  
32 indicating a close relationship between local hydroclimate and atmospheric convective processes related  
33 to the South American Monsoon System.

34

35 **Keywords:**  $\delta^{13}\text{C}$ , speleothem, stalagmite, hydroclimate, South America.



65 Open and closed system models were proposed to explain two extreme cases of dissolution of  
66 calcium carbonate in the percolating solution (Fohlmeister et al., 2011; McDermott et al., 2004; Hendy,  
67 1971). In an open system, the percolating solution remains in equilibrium with the infinite reservoir of  
68 soil CO<sub>2</sub> and, thereby, the bicarbonate in solution receives the δ<sup>13</sup>C fingerprint of this reservoir. Under  
69 these conditions, the contribution of the δ<sup>13</sup>C values from the bedrock to the HCO<sub>3</sub><sup>-</sup> in solution can be  
70 neglected. In a closed system, during the percolation into the epikarst, the solution loses contact with the  
71 soil CO<sub>2</sub>, and the CO<sub>2</sub> in solution is progressively consumed through the dissolution of the bedrock. The  
72 rock dissolution is limited by the initial amount of CO<sub>2</sub> and, consequently, through this process the δ<sup>13</sup>C  
73 from the bedrock influences the isotopic composition of the remaining solution (McDermott, 2004). In  
74 most caves, the interaction between the percolation solution and the host-rock occurs as an intermediate  
75 way between open and closed systems.

76 The δ<sup>13</sup>C values in pedogenic carbonate are closely related to the isotopic values from the  
77 surrounding vegetation (Cerling, 1984; Quade et al., 1989), defined by the plant type (C<sub>3</sub>, C<sub>4</sub> or CAM),  
78 which in turn, will be conditioned by climatic parameters such as temperature, pluviosity, rainfall  
79 seasonality and atmospheric CO<sub>2</sub> (Ehleringer et al., 1997). Vegetation dominated by C<sub>3</sub> plants has δ<sup>13</sup>C  
80 values between -32 ‰ and -20 ‰, while vegetation dominated by C<sub>4</sub> plants is characterized by values  
81 between -17 ‰ to -9 ‰ (Badeck et al., 2005). CAM plants have δ<sup>13</sup>C values that overlap with both C<sub>3</sub> and  
82 C<sub>4</sub> plants. In addition, δ<sup>13</sup>C values of individual C<sub>3</sub> plant species can vary approximately 1 to 2 ‰,  
83 depending on water availability (e.g., Hartman and Danin, 2010). The differences in the δ<sup>13</sup>C values from  
84 total organic matter in soil resulting from the dominant plant types are transferred to stalagmites  
85 precipitated under their respective environment. Thus, stalagmites precipitated in caves under conditions  
86 dominated by C<sub>3</sub> plants typically have values ranging from -14 ‰ to -6 ‰, while those forming below C<sub>4</sub>  
87 plant cover range from -6 ‰ to +2 ‰ (McDermott, 2004; Baker et al., 1997; Dreybrodt, 1988).  
88 Variations in soil δ<sup>13</sup>C values and their evolution over time are controlled by carbon inputs from  
89 vegetation, which is proportional to the organic matter amount and vegetation density; thus denser  
90 vegetation is also associated with more depleted values in soil δ<sup>13</sup>C and vice-versa (Pessenda et al., 2010).  
91 However, the presence of CAM plants can complicate this interpretation since this type of plant present a  
92 large range of δ<sup>13</sup>C values. In addition, the δ<sup>13</sup>C values of C<sub>3</sub> plants are sensitive to atmospheric CO<sub>2</sub>  
93 levels (Van de Water et al., 1994; Schubert and Jahen, 2012), producing a signal that is transferred to  
94 stalagmites (Breecker, 2017).

95 In the cave system,  $\delta^{13}\text{C}$  values from dissolved inorganic carbon (DIC) can undergo fractionation  
96 through prior calcite precipitation (PCP), which is forced by  $\text{CO}_2$  degassing that preferentially removes  
97  $^{12}\text{C}$  from the solution to the cave atmosphere (Mickler et al., 2019), depleting  $^{12}\text{C}$  from the final isotopic  
98 product recorded in stalagmites (Baker et al., 1997). PCP increases during drier periods due to the  
99 increased exposure of seepage solution to air. This can occur during the contact of the solution with air  
100 pockets along the epikarst flow routes and/or with the increase of dripping interval, where the solution is  
101 exposed to the cave air for longer time at the stalactites; both results in  $\text{CO}_2$  degassing from the solution,  
102 promoting the carbonate precipitation in the epikarst and/or stalactites with higher  $\delta^{13}\text{C}$  values (Fairchild  
103 and Baker, 2012). Therefore, the variations in the PCP rate are climate related. In monsoonal climates,  
104 such as in (sub)tropical South America, the amount effect is the dominant process that affects the  $\delta^{18}\text{O}$   
105 value of rainwater, such that an increase in the amount of rainfall results in waters with lower  $\delta^{18}\text{O}$  values  
106 (Vuille et al., 2012). This increase in rainfall amount might also cause a decrease in the  $\delta^{13}\text{C}$  value of  
107 speleothem calcite, by increasing the soil moisture content and soil respiration rates or by reducing PCP,  
108 resulting in a positive correlation between the  $\delta^{18}\text{O}$  and  $\delta^{13}\text{C}$  values of speleothem calcite/aragonite (Cruz  
109 et al., 2006; Mickler et al., 2006; and references therein). While  $\delta^{13}\text{C}$  and  $\delta^{18}\text{O}$  values may be correlated  
110 for different reasons, high correlation between both isotopic ratios can also be indicative of forced kinetic  
111 fractionation, since carbon and oxygen are fractionated in the same direction in this process (Hendy et al.,  
112 1971). The isotopic disequilibrium increases with enhanced ventilation of the cave, which depends on the  
113 temperature gradient between the air inside and outside of the cave. However, the range of values  
114 resulting from the fractionation factor between  $\text{CaCO}_3$  and  $\text{HCO}_3^-$  in tropical temperatures of 15 – 30 °C  
115 has been documented to be  $< 0.5 \text{‰}$  (Polag et al., 2010 and references therein). Recently, Fohlmeister et  
116 al. (2020), using a large dataset of  $\delta^{13}\text{C}$  values in stalagmites deposited post-1900 CE, show evidence for  
117 a temperature control on this proxy, likely driven by vegetation and soil processes, while PCP can explain  
118 the wide  $\delta^{13}\text{C}$  range observed for concurrently deposited samples from the same cave.

119

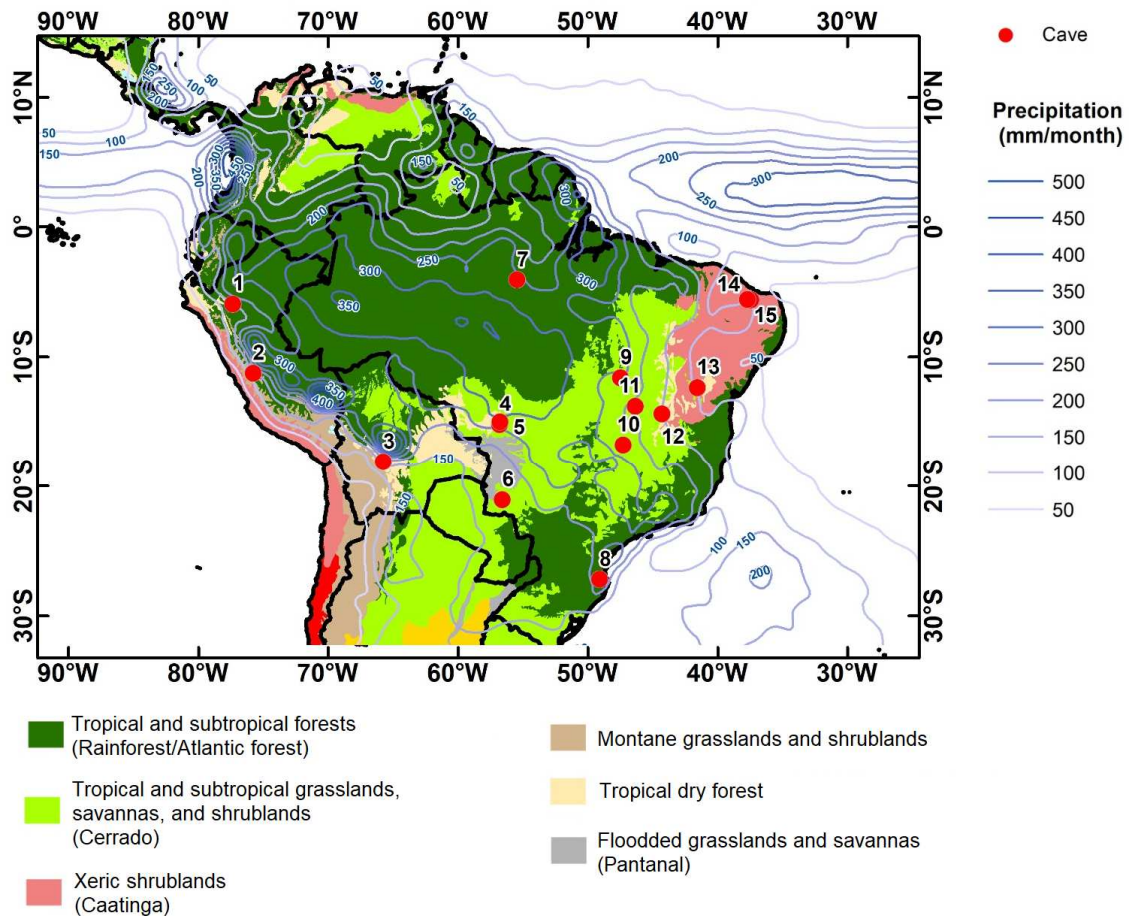
## 120 **2.2 Processes controlling the $\delta^{13}\text{C}$ values in speleothems from South America**

121 The main mode of climate variability in tropical South America is defined by the SAMS  
122 behavior, which also influences vegetation changes. Most of the  $\delta^{18}\text{O}$  records from stalagmites in South  
123 America show a weak monsoon activity during the Medieval Climate Anomaly (MCA, 900-1100 years  
124 CE), in contrast with a strong activity during the Little Ice Age (LIA, 1600-1850 years CE) (Bird et al.,

125 2011; Vuille et al., 2012; Novello et al., 2016; 2018). During the LIA period, a moisture dipole was  
126 documented between the eastern and western portions of tropical South America, due to the displacement  
127 of the South Atlantic Convergence Zone (SACZ) toward the southwest (Campos et al., 2019; Novello et  
128 al., 2018). This change in climate is still not investigated with the  $\delta^{13}\text{C}$  values in stalagmites.

129 Few studies focused on the  $\delta^{13}\text{C}$  values from speleothems in South America. Cruz et al. (2006)  
130 interpreted the  $\delta^{13}\text{C}$  from Botuverá cave (southeastern Brazil, point 8 in Fig. 1) as a proxy for soil  $\text{CO}_2$   
131 productivity, which is modulated at orbital time scales by changes in local temperature brought about by  
132 shifts between summer monsoonal and winter extratropical circulation. Novello et al. (2019) reported a  
133 decrease of 9 ‰ in the  $\delta^{13}\text{C}$  values from Jaraguá cave (point 6 in Fig. 1) during the transition between the  
134 last Glacial and the Holocene periods, resulting from a combination of changes above the cave, including:  
135 changes in the predominant vegetation type from  $\text{C}_4$  to  $\text{C}_3$ , increase of organic matter and soil horizons,  
136 which were mainly caused by the increase in temperature and atmospheric  $\text{CO}_2$ . For the last two  
137 millennia, Jaqueto et al. (2016) show that the concentration of magnetic minerals and  $\delta^{13}\text{C}$  values in the  
138 ALHO6 stalagmite from Pau d'Alho cave (point 4 in Fig. 1) is governed by soil dynamics and changes in  
139 vegetation cover above the cave. Dry periods are associated with less stable soils, resulting in high  
140 erosion and increased mineral flux into karst systems, which occurs simultaneously with increasing  $\delta^{13}\text{C}$   
141 values. Conversely, wetter periods with low  $\delta^{13}\text{C}$  values are associated with soils topped by denser  
142 vegetation that retains micrometer-scale pedogenic minerals and thus reduces detrital fluxes into the cave.  
143 Azevedo et al. (2019) further explored the relationship between  $\delta^{13}\text{C}$  and  $\delta^{18}\text{O}$  during the last millennium  
144 in a speleothem (MV3) from the Brazilian Central region (point 9 in Fig. 1), where wetter (drier) periods  
145 are also associated with lower (higher) values of  $\delta^{18}\text{O}$  and  $\delta^{13}\text{C}$  and higher (lower) speleothem growth  
146 rates. The same interpretation was utilized for the  $\delta^{13}\text{C}$  values of the stalagmites from Tamboril cave,  
147 located further south (point 10 in Fig. 1). However, at this site the  $\delta^{18}\text{O}$  and  $\delta^{13}\text{C}$  do not co-vary, which  
148 the authors interpret as a result of the decoupling between the local hydroclimate and SAMS, documented

149 by the  $\delta^{13}\text{C}$  and  $\delta^{18}\text{O}$ , respectively (Wortham et al., 2017).



150

151 **Fig. 1.** Map of tropical South America with vegetation types (Olson et al., 2001), the main biomes, precipitation (blue  
152 isolines - mm/month, derived from the annual mean for the period from 1998 to 2017, with data from TRMM 3b43 –  
153 Huffman et al., 2014) and location of the study sites from the  $\delta^{13}\text{C}_{2k\_SA}$  dataset. 1- Huagapo cave; 2- Palestina  
154 cave; 3- Umajalanta–Chiflonkhakha; 4- Pau d’Alho cave; 5- Curupira cave; 6- Járuguá cave; 7- Paraiso cave; 8-  
155 Botuverá cave; 9- Mata Virgem cave; 10- Tamboril cave; 11- São Matheus and São Bernardo cave system; 12- Anjos  
156 cave; 13- Diva, Torrinha, Lapa Doce caves; 14- Furna Nova cave; 15- Trapiá cave.  
157

158 The global increase of the atmospheric  $\text{CO}_2$  concentration and temperature likely also influenced  
159 the  $\delta^{13}\text{C}$  values of stalagmites during the last century. Since 1850 the land surface air temperature  
160 increased by about 1.44 °C (Jia et al., 2019), affecting the fractionation between the seepage solution and  
161 the carbonate precipitated inside the caves (Lachniet, 2009), as well as promoting changes in cave  
162 ventilation (Baldini et al., 2008). Furthermore, depleted isotopic carbon has been emitted into the  
163 atmosphere due to the burning of fossil fuels, thereby decreasing the atmospheric  $\delta^{13}\text{C}$  that is transferred  
164 to vegetation. The increase of atmospheric  $\text{CO}_2$  can also favor the flourishing of  $\text{C}_3$  plants, which are less  
165 adapted than  $\text{C}_4$  plants to low atmospheric  $\text{CO}_2$  concentrations (Ehleringer et al., 1997).

166

167 **3 Data Material and Methods**

168 **3.1  $\delta^{13}\text{C}$  data**

169 The dataset used in this study comprises 25 speleothem  $\delta^{13}\text{C}$  records, of which 13 were hitherto  
170 unpublished.  $\delta^{18}\text{O}$  records and chronological models have been published for all stalagmite records. Data  
171 from the published records were obtained from the supplementary material of the respective papers or  
172 downloaded from the NOAA speleothem database ([http://www.ncdc.noaa.gov/data-](http://www.ncdc.noaa.gov/data-access/paleoclimatology-data/datasets/speleothem)  
173 [access/paleoclimatology-data/datasets/speleothem](http://www.ncdc.noaa.gov/data-access/paleoclimatology-data/datasets/speleothem)). Our main goal with this study is to introduce new  
174 cave records to the speleothem community and contextualize their interpretation in a regional framework  
175 for South America during the last two millennia. For that, we used only datasets that were available to us  
176 with speleothem  $\delta^{13}\text{C}$  data from the last two thousand years (since year 0 CE). Therefore, we only  
177 consider this time period for the analyses presented here. All records used, including their references,  
178 cave names, locations and climatic parameters, are listed in Table 1. They are composed of 11,601  $\delta^{13}\text{C}$   
179 values from 25 speleothems, published in 15 different papers (Table 1).

180

181

182

183

184

185

186

187

188

189

190

191

Stalagmite	Cave	Latitude °N	Longitude °E	Reference	Annual Precipitation (mm)	Mean annual T (°C)	Elevation (m.a.s.l)
JAR4	Jaraguá	-21.08	-56.58	Novello et al. (2018; 2019) This study	1400	21.4	570
JAR1	Jaraguá	-21.08	-56.58	Novello et al. (2018) This study	1400	21.4	570
SBE3	São Bernardo	-13.81	-46.35	Novello et al. (2018); Moquet et al. (2016) This study	1270	23.0	630
SMT5	São Matheus	-13.81	-46.35	Novello et al. (2018) This study	1270	23.0	630
ALHO6	Pau d'Alho	-15.21	-56.8	Novello et al. (2016) Jaqueto et al. (2016)	1440	25.5	340
CUR4	Curupira	-15.02	-56.78	Novello et al. (2016) This study	1440	25.5	340
DV2	Diva	-12.37	-41.57	Novello et al. (2012) This study	700	24.5	480
TR5	Torrinha	-12.37	-41.57	Novello et al. (2012) This study	700	24.5	480
LD12	Lapa Doce	-12.37	-41.57	Novello et al. (2012) This study	700	24.5	480
TRA7	Trapiá	-5.59	-37.70	Utida et al. (2020)	700	28.0	72
FN1	Furna Nova	-5.60	-37.44	Cruz et al. (2009) Utida et al. (2020)	700	28.0	100
TM0	Tamboril	-16.80	-47.27	Wortham et al. (2017)	1400	22.5	600
ANJOS1	Lapa dos Anjos	-14.39	-44.30	Stríkis (2015) This study	940	23.7	640
BTV21a	Botuverá	-27.21	-49.09	Bernal et al. (2016) This study	1400	22.0	200
PAR3	Paraiso	-4.07	-55.45	Wang et al. (2017)	2400	26.0	60
PAR1	Paraiso	-4.07	-55.45	Wang et al. (2017)	2400	26.0	60
MV3	Mata Virgem	-11.62	-47.49	Azevedo et al. (2019)	1570	26.8	365
POO-H1	Huagapo	-11.27	-75.79	Kanner et al. (2013)	459	10.4	3800
P09-H2	Huagapo	-11.27	-75.79	Kanner et al. (2013)	459	10.4	3800
BOTO3	Umajalanta– Chiflonkhakha	-18.12	-65.77	Apaéstegui et al. (2018) This study	518	17.0	2650
BOTO7	Umajalanta– Chiflonkhakha	-18.12	-65.77	Apaéstegui et al. (2018) This study	518	17.0	2650
BOTO10	Umajalanta– Chiflonkhakha	-18.12	-65.77	Apaéstegui et al. (2018) This study	518	17.0	2650
BOTO1	Umajalanta– Chiflonkhakha	-18.12	-65.77	Apaéstegui et al. (2018) This study	518	17.0	2650
PAL3	Palestina	-5.92	-77.35	Apaéstegui et al. (2014)	1570	22.8	870
PAL4	Palestina	-5.92	-77.35	Apaéstegui et al. (2014)	1570	22.8	870

192 **Table 1.** Caves, locations and regional characteristics. Information obtained from the original papers.

193

### 194 3.2 Stalagmites and regional settings

195 As presented in the original papers, all speleothems used in this study were collected with the  
196 initial goal to reconstruct the SAMS using the  $\delta^{18}\text{O}$  values. Therefore, stalagmites with a candle-type  
197 shape and uniform growth were preferentially collected in isolated chambers located far from the cave  
198 entrance. At such locations, temperature displays only minor variations throughout the year (characteristic  
199 of tropical caves), the air circulation is restricted,  $\text{CO}_2$  concentrations are higher than atmospheric values,  
200 and the air is saturated in humidity. These conditions minimize the seasonal effects of ventilation and  
201 temperature, degassing and overall kinetic effects on the isotopic composition of the stalagmites.

202           The speleothem  $\delta^{13}\text{C}$  records used here are distributed throughout tropical South America (Fig.  
203 1), covering a region spanning the latitudes 4 °S to 21 °S and longitudes 42 °W to 76 °W. The domain  
204 comprises the following climates (according to the Köppen climate classification): monsoon (Am),  
205 tropical savanna (Aw), warm semi-arid (BSh) and humid subtropical (Cwa). The annual precipitation  
206 amount ranges from 450 to 2400 mm, mainly related to the SAMS and its subcomponent the SACZ  
207 (Novello et al., 2018). The equatorial portion is also under direct influence of the Intertropical  
208 Convergence Zone (ITCZ). Except for the sites located in the Andes, all records are located at altitudes  
209 below 700 m.a.s.l. (Table 1). At these lowland sites, precipitation amount and the length of the rainy  
210 season define the three main vegetation types (Fig. 1). High precipitation amounts that are well  
211 distributed over the year are typical of Tropical Forest, while Caatinga is characterized by an environment  
212 with lower precipitation, concentrated during a few months. Cerrado, the main biome of central South  
213 America, presents hydrological conditions in-between these two end-members. In general, temperature  
214 decreases with increasing latitude and altitude; the mean annual temperature in the lowlands ranges from  
215 21.4 to 26.8 °C, while the sites in the Andes reach temperatures around 10 °C (Table 1).

216

### 217 **3.3 Methods**

218           To assess the shared variance among the  $\delta^{13}\text{C}$  records from the different cave sites, while  
219 considering the stalagmites' age uncertainties, we employ a Monte-Carlo Principal Component Analysis  
220 (MC-PCA) as described in Campos et al. (2019), which consists of the following steps: (1) A linear age-  
221 depth model was constructed for each record, accounting for the  $\pm 1\sigma$  standard deviations in the dating  
222 uncertainty through a set of 1000 Monte-Carlo simulations, which resulted in 1000 age models for each  
223 isotopic sample. The corresponding isotopic time series are obtained through linear interpolation between  
224 ages using the age-depth model (Deininger et al., 2017); (2) Stalagmite records from the same karst  
225 region were merged into a single time series by synchronizing the time series using a cubic spline during  
226 the overlap period, and each time series was normalized to unit variance (z-scores) before they were  
227 averaged into one time series; (3) The time series were reconstructed using the inversion of the  
228 normalization of the longer time series (using standard deviation and the mean of the longer time series);  
229 (4) The time series were resampled to annual resolution before being low-pass filtered at the band of 1/30  
230 years<sup>-1</sup>; (5) From the 1000 Monte-Carlo age model simulations, one time series is randomly chosen from

231 each record, generating a set of time series; the Principal Component Analysis (PCA) is then performed  
232 over this set of data. This procedure is repeated 1000 times, in such a way that all the simulations are  
233 being used, generating a set of spatial patterns (or loadings), principal components (or scores) and  
234 eigenvalues (containing the explained variance of the spatial pattern and principal component). These  
235 analyses were carried out in Matlab with codes written using its native routines.

236 The MC-PCA was focused on the time period between 650 and 1950 CE because this is the time  
237 interval covered by most sites. This procedure resulted in a set of ten time series, each corresponding to a  
238 site shown in Fig. 3: Jar (composed by JAR1 + JAR4), SBE (composed by SBE3 + SMT5), ALH  
239 (composed by ALHO6 + CUR4), DV2 (composed by DV2 + TR5 + LD12), TMO (composed only by  
240 TMO), ANJ (composed only by ANJOS1), PAR (composed by PAR1 + PAR3), HUA (composed by  
241 P00-H1 + P09-H2), BOTO (composed by BOTO1 + BOTO3 + BOTO7 + BOTO10) and PAL (composed  
242 by PAL3 + PAL4). Four stalagmites presented in Fig. 1 (MV3, FN1, TRA7, BTV21a) were not included  
243 in the PCA because these records cover only a limited time period and no other stalagmites from the same  
244 karst systems exist that could be merged, or because their data resolution is significantly lower (more than  
245 15 years between individual data points in the geochronological model).

246 Regression analyses between the  $\delta^{13}\text{C}$  data and other parameters were performed using the data  
247 presented in Table 1 and 2 to test possible climatic influences on the  $\delta^{13}\text{C}$  values from stalagmites. Many  
248 stalagmites from this study experience similar precipitation amounts and/or temperature. Hence, we  
249 used a single averaged  $\delta^{13}\text{C}$  value for the stalagmites that are located within regions that experience  
250 similar precipitation amount or temperature (listed in Table 1) to provide regression analysis tests: “ $\delta^{13}\text{C}$   
251 vs. precipitation amount” and “ $\delta^{13}\text{C}$  vs. temperature”. Precipitation and temperature values that fall within  
252 a range of 50 mm and 1°C, respectively, were considered as similar. This approach results in one  $\delta^{13}\text{C}$   
253 value per climatic region entering the regression model, ensuring that climatic regions where stalagmites  
254 are more common are not overrepresented and therefore do not lead to regionally biased results. Sites  
255 from the high-altitude Andes (Umajalanta–Chiflonkhakha and Huagapo cave systems) were excluded in  
256 the correlation and regression analyses, as these sites introduce large outliers due to the differences in  
257 altitude and temperature, that would equally bias the results. The average  $\delta^{13}\text{C}$  value over the last two  
258 millennia was used in the analysis, which allows us to use all stalagmites to provide a spatially more  
259 complete picture of the records from South America and minimize possible inconsistencies in the data  
260 related to geochronology and resolution. Restricting the analysis to only modern  $\delta^{13}\text{C}$  values would be

261 limiting the use of our dataset since only a few stalagmites present data from the last 50 years. In theory,  
262 the recent  $\delta^{13}\text{C}$  values should be more closely related to current temperature and precipitation. However,  
263 as is shown in Fig. 2 and discussed in sections 4 and 5, using the  $\delta^{13}\text{C}$  averaged over the full record still  
264 results in a high  $R^2$  with high statistical significance ( $p < 0.01$ ) of the relationship between  $\delta^{13}\text{C}$  and  
265 climatic parameters, which suggest that average  $\delta^{13}\text{C}$  values over the last two millennia are indeed  
266 representative of the current climatic conditions.

267 To establish the correlation between the  $\delta^{13}\text{C}$  and the growth rate from speleothems, we  
268 calculated the growth rate based on the length of the interval between two consecutive U/Th ages and  
269 used the mean  $\delta^{13}\text{C}$  value, averaged over the respective interval.

270

#### 271 **4 Results**

272 The  $\delta^{13}\text{C}$  values from the  $\delta^{13}\text{C}_{2k\_SA}$  dataset range from -11.5 to 6.8 ‰, although the vast  
273 majority of the data lie within -11 and -1 ‰ (Figures 1 to 25 in supplementary material). The highest  
274 values and largest variability stem from the TR5 stalagmite, ranging from -3.8 to 6.8 ‰ (amplitude of 10  
275 ‰), which contrasts with the average amplitude of 4.5 ‰ from the other stalagmites.

276 The coefficient of determination ( $R^2$ ) between the time series of  $\delta^{18}\text{O}$  and  $\delta^{13}\text{C}$  was calculated for  
277 each stalagmite and is listed in Table 2. The highest coefficient of determination ( $r^2$ : 0.96,  $p < 0.01$ ) is  
278 displayed by the TR5 stalagmite, while the average  $r^2$  of the  $\delta^{13}\text{C}_{2k\_SA}$  dataset is 0.29. Average  $\delta^{13}\text{C}$   
279 values from the speleothems display a high negative correlation with the annual mean precipitation  
280 amount ( $r^2$ : 0.67,  $p < 0.01$ ) and a weaker, positive correlation with temperature ( $r^2$ : 0.45,  $p < 0.05$ ) of their  
281 respective regions (Fig. 2). No significant correlation was found with altitude ( $p > 0.05$ ). The relationships  
282 between the growth rate and average  $\delta^{13}\text{C}$  values are statistically significant ( $p \leq 0.05$ ) only in the  
283 stalagmites JAR4 ( $r^2$ : 0.21), DV2 ( $r^2$ : 0.50), TR5 ( $r^2$ : 0.75), LD12 ( $r^2$ : 0.70) and TRA7 ( $r^2$ : 0.20), all with  
284 negative slopes (Table 2).

285

286

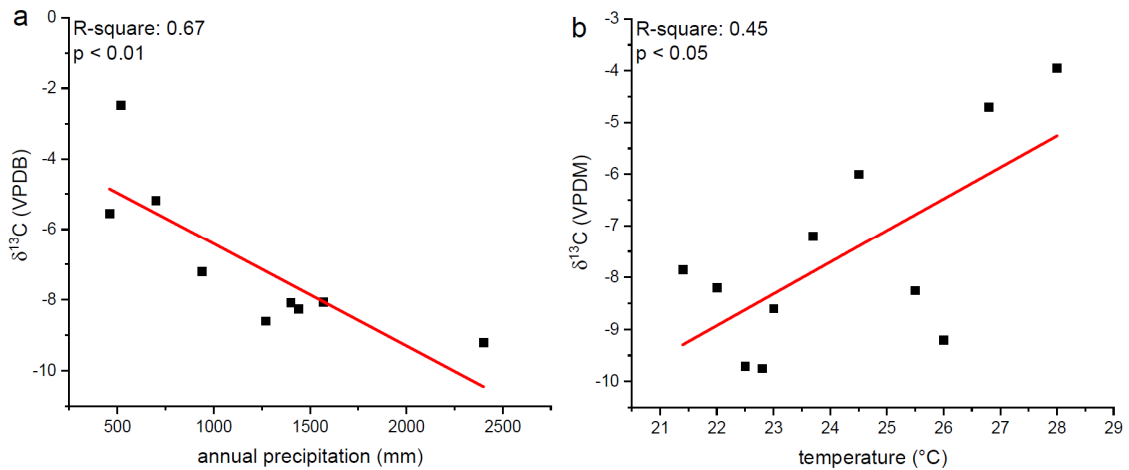
287

288

Stalagmite	$\delta^{18}\text{O}$ mean	$\delta^{13}\text{C}$ mean	$R^2$ $\delta^{18}\text{O} \times \delta^{13}\text{C}$	Time period covered (years BP)	Isotopic data points	Mean resolution (years)	$R^2$ Growth rate $\times \delta^{13}\text{C}$	$\delta^{13}\text{C}$ of the main rock formation	Host geology
JAR4	-4.8	-8.5	0.50 (p<0.01)	-50 to 760	237	3.4	<b>(-) 0.21 (p=0.05)</b> , n° of segments: 18	1* (1)	Bocaina Fm, Corumba Group (Neoproterozoic)
JAR1	-3.8	-7.2	0.21 (p<0.01)	499 to 1508	318	3.2	(+) 0.24 (p=0.17), n° of segments: 9	1* (1)	Bocaina Fm Corumba Group (Neoproterozoic)
SBE3	-4.3	-8.9	0.04 (p<0.01)	-60 to 827	1710	0.5	(+) 0.29 (p=0.12), n° of segments: 10	-5.5 to -3 (2)	Urucua Fm, Mata da Corda Group (Cretaceous)
SMT5	-4.2	-8.3	0.13 (p<0.01)	749 to 1686	575	1.6	(-) 0.35 (p=0.60), n° of segments: 3	-5.5 to -3 (2)	Urucua Fm, Mata da Corda Group (Cretaceous)
ALHO6	-6.2	-6.6	0.57 (p<0.01)	90 to 1458	1169	1.2	(+) 0.03 (p=0.63), n° of segments: 11	-5 to 0 (3)	Guia Fm, Araras Group (Neoproterozoic)
CUR4	-7.6	-9.9	0.25 (p<0.01)	-21 to 155	252	0.7	(+) 0.00 (p=0.94), n° of segments: 7	-5 to 0(3)	Guia, Araras Group (Neoproterozoic)
DV2	-3.7	-9.2	0.35 (p<0.01)	39 to 2765	538	5.0	<b>(-) 0.50 (p=0.02)</b> , n° of segments: 10	-9 to +10 (4)	Salitre Fm, Una Group (Neoproterozoic)
TR5	-2.9	-1.1	0.96 (p<0.01)	-57 to 76	90	1.5	<b>(-) 0.75 (p&lt;0.01)</b> , n° of segments: 7	-9 to +10 (4)	Salitre Fm, Uma Group (Neoproterozoic)
LD12	-3.2	-7.7	0.35 (p<0.01)	-61 to 39	122	0.8	<b>(-) 0.70 (p=0.04)</b> , n° of segments: 6	-9 to +10 (4)	Salitre Fm, Una Group (Neoproterozoic)
TRA7	-2.8	-3.0	0.05 (p<0.01)	17 to 5507	818	6.4	<b>(-)0.20 (=0.03)</b> , n° of segments: 23	0* (5)	Jandaíra Fm, Apodi Group (Cretaceous)
FN1	-2.3	-4.9	0.87 (p<0.03)	-54 to 2275	88	26.5	X, n° of segments: 3	0* (5)	Jandaíra Fm, Apodi Group (Cretaceous)
TM0	-5.4	-9.7	0.24 (p<0.01)	-32 to 1678	471	3.6	0.00 (p=0.87), n° of segments: 12	-5 to +16 (6)	Sete Lagos Fm, Bambuí Group (Neoproterozoic)
ANJOS1	-3.7	-7.2	0.09 (p<0.01)	-57 to 2927	1272	2.4	0.00 (p=0.72), n° of segments: 26	-5 to +2 (7)	Sete Lagoas Fm. Bambuí Group (Neoproterozoic)
BTV21a	-3.8	-8.2	0.03 (p<0.01)	196 to 9211	230	39.2	X, n° of segments: 3	X	Botuverá Fm, Brusque Group (Neoproterozoic)
PAR3	-5.7	-8.9	0.42 (p<0.01)	-48 to 768	144	5.7	(-) 0.26 (p=0.24), n° of segments: 7	-2.2 to 5.2 (8)	Itaituba Fm Tapajos Group (Paleozoic)
PAR1	-6.6	-9.5	0.00 (p<0.44)	714 to 4812	449	9.1	X, n° of segments: 3	-2.2 to 5.2 (8)	Itaituba Fm Tapajos Group (Paleozoic)
MV3	-1.9	-4.7	0.45 (p<0.01)	250 to 1032	537	1.4	(-) 0.46 (p=0.10), n° of segments: 7	X	Mato Virgem Fm, Natividade Group (Precambrian)
P00-H1	-13.3	-5.9	0.24 (p<0.01)	-50 to 1391	289	5.0	(+) 0.55 (p=0.26), n° of segments: 4	X	Aramachay Fm, Pucara Group (Triassic)
P09-H2	-13.0	-5.2	0.20 (p<0.01)	1099 to 7146	1272	5.7	(-) 0.35 (p=0.29), n° of segments: 4	X	Aramachay Fm, Pucara Group (Triassic)
Boto3	-9.7	-1.7	0.26 (p<0.01)	171 to 1242	256	4.0	<b>(-) 0.94 (p=0.01)</b> , n° of segments: 8	X	Miraflores Fm, Pucara Group (Cretaceous)
Boto7	-10.8	-3.9	0.00 (p=0.6)	78 to 388	97	1.8	X, n° of segments: 2	X	Miraflores Fm, Pucara Group (Cretaceous)
Boto10	-9.7	-3.1	0.34 (p<0.01)	543 to 1217	207	3.3	(+) 0.36 (p=0.40), n° of segments: 3	X	Miraflores Fm, Pucara Group (Cretaceous)
Boto1	-10.2	-1.2	0.41 (p<0.01)	218 to 383	20	7.9	X, n° of segments: 1	X	Miraflores Fm, Pucara Group (Cretaceous)
PAL3	-7.1	-10.1	0.00 (p=0.2)	21 to 850	192	4.3	(+) 0.65 (p=0.10), n° of segments: 4	X	Chambara Fm, Pucara Group (Triassic_Jurassic)
PAL4	-7.1	-9.4	0.25 (p<0.01)	151 to 1536	248	5.4	(+) 0.12 (p=0.27), n° of segments: 11	X	Chambara Fm, Pucara Group (Triassic_Jurassic)

289 **Table 2:** Stalagmites and their respective data information. Coefficients of determination ( $R^2$ ) between growth rate and  $\delta^{13}\text{C}$  values was calculated based on the length interval between ages and  
290 the mean  $\delta^{13}\text{C}$  values of each interval. Confidence levels at this column equal to or higher than 95% (p≤0.05) are shown in bold and the signal “+” and “-” denotes positive and negative slopes,  
291 respectively. (1) Novello et al. (2019); (2) Lima (2011); (3) Nogueira et al. (2006); (4) Caird et al. (2017); (5) Utida et al. (2020); (6) Alvarenga et al. (2014); (7) Caetano-Filho et al. (2019); (8)  
292 Campos (2013). (\*) Site where the  $\delta^{13}\text{C}$  values were measured in the bedrock that hosts the cave.

293

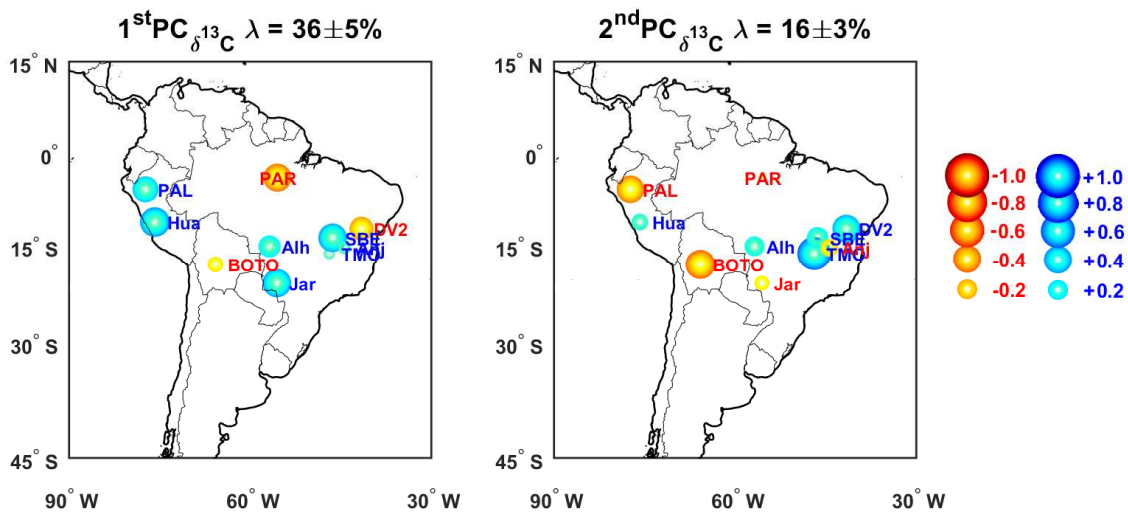


294

295 **Fig. 2.** Relationship between the  $\delta^{13}\text{C}$  from the  $\delta^{13}\text{C}_{2k\_SA}$  dataset with annual precipitation (a) and annual mean  
 296 temperature (b) of each study site.

297

298 The MC-PCA methodology was applied to the full  $\delta^{13}\text{C}_{2k\_SA}$  dataset. The first principal  
 299 component (PC1) explained  $\sim 36\%$  of the total variance (Fig. 3 and 4). Positive loadings are associated  
 300 with the  $\delta^{13}\text{C}$  records from the caves Huagapo (Hua), Palestina (PAL), Jaraguá (Jar), and the merged  
 301 records from the caves Pau d'Alho/Curupira (Alh) and São Bernardo/São Matheus (SBE), whereas  
 302 negative loadings are linked to the records from the caves Diva de Maura/Torrinha/Lapa Doce (DV2),  
 303 Paraiso caves (PAR) and Umajalanta–Chiflonkhakha (BOTO) (Fig. 3), indicating out of phase  $\delta^{13}\text{C}$   
 304 variability between the two cave site groups. Positive values characterize the time interval of  $\sim 600$ – $1500$   
 305 CE in PC1, while negative values are predominant during the period  $\sim 1500$ – $1950$  CE, with an incursion  
 306 to more negative values centered at  $\sim 1180$  CE (Fig. 4). PC2 explained  $\sim 16\%$  of the variance, with large  
 307 positive loadings displayed by the records located in central Brazil, especially the TM0 and DV2 records,  
 308 whereas large negative loadings are displayed by the records from high altitudes (PAL and BOTO). The  
 309 other study sites present low and variable contributions for PC2.



310

311 **Fig. 3.** Maps of South America with the main loadings of the Principal Component Analysis (PCA) and explained  
 312 total variance. Blue and red dots represent positive and negative loadings, respectively. The magnitude of the  
 313 loadings is represented by the size of the dots. The larger the dot, the more representative it's loading is of the  
 314 respective PC.

315

## 316 5 Discussion

317 The host-rocks of the caves in this study are predominantly of Neoproterozoic age, located in the  
 318 Brazilian shield (Table 2). Isotopic studies carried out in these carbonate rock sequences show a wide  
 319 range of values, varying between  $\sim -5$  to  $16$  ‰ within the same rock unit or even the same outcrop (Table  
 320 2). The absence of isotopic studies in the same bedrock where the caves are located, precludes a precise  
 321 quantification of the influence of these different rock sequences on the  $\delta^{13}\text{C}$  values of the stalagmites. Of  
 322 the study sites presented here, the  $\delta^{13}\text{C}$  from its host-rock was only measured at Jaraguá and Trapiá caves  
 323 (Novello et al., 2019; Utida et al., 2020). In both sites, more positive  $\delta^{13}\text{C}$  values close to bedrock values  
 324 were reported in their stalagmites during periods of sparse vegetation and thin soil layers above the caves.  
 325 Although both papers are describing environmental changes at orbital timescales, nowadays these are the  
 326 typical characteristics of the sites Huagapo, Umajalanta–Chiflonkhakha, Mata Virgem, Trapiá and  
 327 Torrinha; all featuring stalagmites with high  $\delta^{13}\text{C}$  values (Table 2). Aside from the stalagmites of these  
 328 sites and ALHO6, all other stalagmites have  $\delta^{13}\text{C}$  values lower than  $-6$  ‰ throughout the last two  
 329 millennia, indicating the predominance of thick soil with higher organic matter content from the regions  
 330 of Cerrado and/or Tropical Forest.  $\delta^{13}\text{C}$  values below  $-6$  ‰ in stalagmites are also considered indicative of  
 331 predominance of  $\text{C}_3$  plants above the caves in geochemical models (McDermott, 2004; Baker et al., 1997;

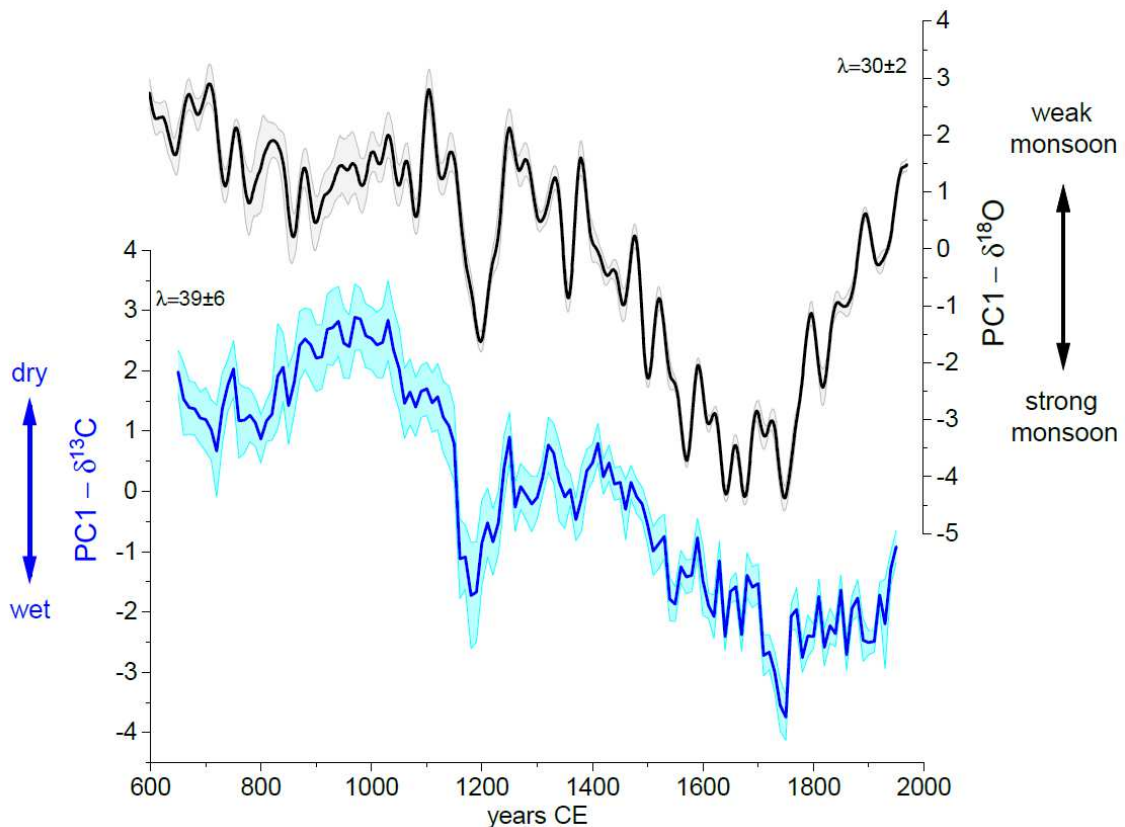
332 Dreybrodt, 1988), if considering bedrock with  $\delta^{13}\text{C}$  values around +1 ‰ (which is the average value for  
333 South American carbonates, Table 2).

334 TR5 presents  $\delta^{13}\text{C}$  values that are significantly higher than all other samples, and the abrupt  
335 increase in  $\delta^{13}\text{C}$  occurs just before the complete stop of carbonate deposition at ~1920 CE and ~2006 CE  
336 (Table 2), both of which are periods of predominantly dry conditions in the region (Novello et al., 2012).  
337 High values followed by an abrupt decrease also occur after the depositional hiatus at ~1960 CE. The  $r^2$   
338 between  $\delta^{13}\text{C}$  and  $\delta^{18}\text{O}$  is close to 1 (Table 2), which indicates that both isotopes underwent fractionation  
339 together in this sample. These results support the notion that the TR5 stalagmite was precipitated under  
340 strong kinetic effects due to high evaporation rates and/or significantly reduced dripping rates (resulting  
341 in a long time period for isotope re-equilibration between solution and cave atmosphere) at the moment of  
342 carbonate precipitation, which is accentuated during drier periods, culminating in a complete halt of  
343 carbonate precipitation. Although the kinetic effect might be the main factor responsible for the high  
344 amplitude and isotopic values in TR5, this stalagmite still preserves paleoclimate information regarding  
345 the  $\delta^{18}\text{O}$  in precipitation that co-varies with the  $\delta^{18}\text{O}$  from other stalagmites in the region, as well as with  
346 pluviometric data from meteorological stations (Novello et al., 2012).

347 Most of the stalagmites from the  $\delta^{13}\text{C}_{2k\_SA}$  dataset feature coefficients of determination  
348 between their  $\delta^{13}\text{C}$  and  $\delta^{18}\text{O}$  values ranging from 0.20 to 0.56 (Table 2). The  $\delta^{18}\text{O}$  values in stalagmites  
349 from tropical South America covering the last 2000 years have been interpreted as a proxy of the intensity  
350 of the SAMS (Azevedo et al., 2019; Novello et al., 2012, 2016, 2018; Apaéstegui et al., 2014; 2018;  
351 Wortham et al., 2017; Vuille et al., 2012) and the SACZ, a continuous band of low-level wind  
352 convergence and precipitation that extends in a northwest-southeast direction across southeastern South  
353 America (Novello et al., 2018). Since an increase in local rainfall promotes a decrease of PCP, an increase  
354 of gas  $\text{CO}_2$  derived from soil organic matter and favors  $\text{C}_3$  plants over  $\text{C}_4$  plants (all processes that result  
355 in decreasing  $\delta^{13}\text{C}$  values in stalagmites), we argue that a correlation between  $\delta^{13}\text{C}$  and  $\delta^{18}\text{O}$  values is the  
356 result of a close relationship between local hydroclimate and atmospheric convective processes (inferred  
357 by  $\delta^{18}\text{O}$ ). This hypothesis is supported by the existing correlation between the annual rainfall amount and  
358 the average  $\delta^{13}\text{C}$  values of the stalagmites ( $r^2$ : 0.67, Fig. 2), and by the PC1 loadings derived from the  
359  $\delta^{13}\text{C}_{2k\_SA}$  dataset (Fig. 3), showing a very similar spatial distribution as those displayed in PC1 derived  
360 from the  $\delta^{18}\text{O}$  dataset from speleothems over tropical South America by Campos et al. (2019). Both PC1-  
361  $\delta^{13}\text{C}$  and PC1- $\delta^{18}\text{O}$  show positive loadings for the locations to the southwest of the SACZ and negatives

362 loadings for those records located to the northeast (Fig. 3), which characterizes the SACZ precipitation  
363 dipole in South America (Campos et al., 2019; Novello et al., 2018). The BOTO site (Fig. 3) is an  
364 exception in this scenario, but this region may have partially been under the influence from a different  
365 climate system with a different moisture source in the past (Apaéstegui et al., 2018). This relationship  
366 between the  $\delta^{13}\text{C}$  and local hydroclimate was already documented for the ALHO6 stalagmite using a  
367 multiproxy approach (Jaqueto et al., 2016).

368



369

370 **Fig. 4.** Comparison between the first Principal component (PC1) derived from the  $\delta^{13}\text{C}_{2k}$  dataset (this study)  
371 representing the main mode of hydroclimate variability and PC1 based on the  $\delta^{18}\text{O}$  from stalagmites from South  
372 America (PC1 -  $\delta^{18}\text{O}$ ) from Campos et al. (2019) representing the main mode of variability of the South American  
373 Monsoon System. The uncertainties associated with the PC1s are shown by the colored and gray shading.  $\lambda$  indicates  
374 the percentage of explained variance by each PC.

375

376 Strong correspondence throughout the time-series between scores of PC1- $\delta^{13}\text{C}$  and PC1- $\delta^{18}\text{O}$   
377 further corroborates the overall coupling between the monsoon and local hydroclimate during the last  
378 ~1400 years (Fig. 4). This coupling ceases after ~1750 CE, when the monsoon weakened at a faster rate  
379 than the local hydrological response. However, the hydrologic variability inferred from PC1- $\delta^{13}\text{C}$  is  
380 biased by vegetation changes, which responds to other influences beyond the local rainfall amount, such

381 as temperature, atmospheric CO<sub>2</sub>, deforestation and fire (parameters that have increased significantly over  
382 the last 250 years).

383 PC2 explains only 16 % of the δ<sup>13</sup>C variability (Fig. 3). It shows large positive loadings at sites  
384 located in lowlands of central Brazil and negative loadings at sites located in the Andes (Fig. 3). This  
385 difference is possibly related to different effects of temperature at different altitudes. Changes in  
386 continental temperature are amplified at higher elevation (Ohmura, 2012), leading to a larger effect on the  
387 δ<sup>13</sup>C values at sites located at higher altitudes, thereby increasing the isotopic differences between sites  
388 located at low and high elevation.

389 Growth rates also show a weak correlation with the δ<sup>13</sup>C values from the δ<sup>13</sup>C\_2k\_SA dataset.  
390 The correlation between the growth rate and δ<sup>13</sup>C values is statistically significant (p-values ≤ 0.05) only  
391 in the stalagmites JAR4, DV2, TR5, LD12 and TRA7 (Table 2). In these stalagmites, all regression  
392 coefficients present a negative slope, which is expected, as a higher growth rate leads to lower δ<sup>13</sup>C values  
393 because the time for isotopic enrichment of the DIC through kinetic effects is reduced during carbonate  
394 precipitation (Fohlmeister et al., 2020).

395

## 396 **6 Conclusions**

397 Here we present a new set of δ<sup>13</sup>C records from speleothems collected over a broad region of  
398 tropical South America. These data were integrated with previously published speleothem δ<sup>13</sup>C records to  
399 characterize the main controls on carbon isotope variations in this region. The predominance of C<sub>3</sub> plants  
400 above most of the karst systems studied here is responsible for the low δ<sup>13</sup>C values (< -6 ‰) in most of  
401 the speleothems, while local hydroclimate associated with PCP process is the main driver behind its  
402 variability during the last two millennia. Unlike what was observed in the global compilation of δ<sup>13</sup>C  
403 records for the period after 1900 CE (Fohlmeister et al., 2020), local temperature and growth rate play a  
404 minor role in shaping the δ<sup>13</sup>C values in the δ<sup>13</sup>C\_2k\_SA dataset. The probable reason for this difference  
405 between studies is that most of the speleothems in our database formed under tropical conditions,  
406 characterized by a limited temperature range, whereas the SISAL\_v1 dataset studied by Fohlmeister et al.  
407 (2020) is biased towards records from high latitudes with a much larger temperature range.

408 Using Monte Carlo Principal Component Analysis, we produce an index of the mean hydrologic  
409 conditions and its changes over tropical South America for the last two millennia, which is closely related  
410 to monsoon variability for the period prior to 1750 CE. The recent break-down in the relationship  
411 between monsoon and local hydroclimate may have been caused by the increase in temperature, CO<sub>2</sub>,  
412 deforestation and fire during the current warm period; however, further studies are required to test this  
413 hypothesis.

414

#### 415 **7 Data availability**

416 The new  $\delta^{13}\text{C}$  records from  $\delta^{13}\text{C}_{2\text{k\_SA}}$  dataset will be available at PANGAEA.

417

#### 418 **References**

419 Alvarenga, C.J.S., Santos, R.V., Vieira, L.C., Lima, Barbara, A.F., Mancini, L.H., 2014. Meso-  
420 Neoproterozoic isotope stratigraphy on carbonates platforms in the Brasilia Belt of Brazil.  
421 *Precambrian. Res.* 251, 164-180. <https://doi.org/10.1016/j.precamres.2014.06.011>.

422 Apaéstegui, J., Cruz, F.W., Vuille, M., Fohlmeister, J., Espinoza, J. C., Sifeddine, A., Strikis, N., Guyot,  
423 J. L., Ventura, R., Cheng, H., Edwards, R.L., 2018. Precipitation changes over the eastern Bolivian  
424 Andes inferred from speleothem (d18O) records for the last 1400 years. *Earth Planet. Sci. Lett.* 494,  
425 124 – 134, <https://doi.org/10.1016/j.epsl.2018.04.048>.

426 Apaéstegui, J., Cruz, F.W., Sifeddine, A., Vuille, M., Espinoza, J.C., Guyot, J.-L., Khodri, M., Strikis, N.,  
427 Santos, R.V., Cheng, H., Edwards, L., Carvalho, E., Santini, W., 2014. Hydroclimate variability of  
428 the northwestern Amazon Basin near the Andean foothills of Peru related to the South American  
429 Monsoon System during the last 1600 years. *Clim. Past*, 10, 1967–1981, [https://doi.org/10.5194/cp-](https://doi.org/10.5194/cp-10-1967-2014)  
430 10-1967-2014.

431 Azevedo, V., Stríkis, N.M., Santos, R.A., Souza, J.G., Ampuero, A., Cruz, F.W., Oliveira, P., Stumpf,  
432 C.F., Vuille, M., Mendes, V.R., Cheng, H., Edwards, R.L., 2019. Medieval Climate Variability in the

433 eastern Amazon-Cerrado regions and its archeological implications. *Sci. Rep.* 9, 20306,  
434 <https://doi.org/10.1038/s41598-019-56852-7>.

435 Badeck, F.W., Tcherkez, G., Nogues, S., Piel, C., Ghashghaie, J., 2015. Post-photosynthetic fractionation  
436 of stable carbon isotopes between plant organs—a widespread phenomenon. *Rapid. Commun. Mass*  
437 *Sp.* 19(11), 1381-1391, <https://doi.org/10.1002/rcm.1912>.

438 Baker, A., Ito, E., Smart, P.L. and McEwan, R.F., 1997. Elevated and variable values of  $\delta^{13}C$  in  
439 speleothems in a British cave system. *Chem. Geol.* 136, 263–270.

440 Baldini, J.U.L., McDermott, F., Hoffmann, D.L., Richards, D.A., Clipson, N., 2008. Very high-frequency  
441 and seasonal cave atmosphere  $PCO_2$  variability: implications for stalagmite growth and oxygen  
442 isotope-based paleoclimate records. *Earth Planet. Sci. Lett.* 272, 118–129,  
443 <https://doi.org/10.1016/j.epsl.2008.04.031>.

444 Bernal, J.P., Cruz, F.W., Stríkis, N.M., Wang, X., Deininger, M., Catunda, M.C.A., Ortega-Obregón, C.,  
445 Cheng, H., Edwards, R.L., Auler, A.S., 2016. High-resolution Holocene South American monsoon  
446 history recorded by a speleothem from Botuverá Cave, Brazil. *Earth Planet. Sci. Lett.* 450, 186-196,  
447 <https://dx.doi.org/10.1016/j.epsl.2016.06.008>.

448 Bird, B.W., Abbott, M.B., Vuille, M., Rodbell, D.T., Stansell, N.D., Rosenmeier, M.F., 2011. A 2,300-  
449 year-long annually resolved record of the South American summer monsoon from the Peruvian  
450 Andes. *Proc. Natl. Acad. Sci.* 108(21), 8583–8588, <http://doi.org/10.1073/pnas.1003719108>.

451 Breecker, D.O., 2017. Atmospheric  $pCO_2$  control on speleothem stable carbon isotope  
452 compositions. *Earth. Planet. Sci. Lett.* 458, 58-68, <https://doi.org/10.1016/j.epsl.2016.10.042>.

453 Caetano-Filho, S., Paula-Santos, G.M., Guacaneme, C., Babinski, M., Babinski, M., Bedoya-Rueda, C.,  
454 Peloso, M., Amorim, K., Afonso, J., Kuchenbecker, M., Reis, H.L.S., Trindade, R.I.F., 2019.  
455 Sequence stratigraphy and chemostratigraphy of an Ediacaran-Cambrian foreland-related carbonate  
456 ramp (Bambuí Group, Brazil). *Precambrian. Res.* 331, 105365.  
457 [doi.org/10.1016/j.precamres.2019.105365](https://doi.org/10.1016/j.precamres.2019.105365).

458 Caird, R.A., Pufahl, P.K., Hiatt, E.E., Abram, M.B., Rocha, A.J.D., Kyser, T.K., 2017. Ediacaran  
459 stromatolites and intertidal phosphorite of the Salitre Formation, Brazil: Phosphogenesis during the

460 Neoproterozoic Oxygenation Event. *Sediment. Geol.* 350, 55-71,  
461 <http://doi.org/10.1016/j.sedgeo.2017.01.005>.

462 Calo, C.M., Cortés, L.I., 2009. A contribution to the study of diet of formative societies in Northwestern  
463 Argentina: isotopic and archaeological evidence. *Int. J. Osteoarchaeol.*, 19, 192-203,  
464 <http://doi:10.1002/oa.1052>.

465 Campos, A.C.P.P., 2013. *Paleoambiente e quimioestratigrafia da formação Itaituba, carbonífero da borda*  
466 *sul da Bacia do Amazonas, região de Uruará – Pará. Amélia Carolina Pimenta Parente de Campos.*  
467 *M. S. thesis, Universidade Federal do Pará, Brazil, 77 pp, 2013.*

468 Campos, J.L.P.S., Cruz, F.W., Ambrizzi, T., Deininger, M., Vuille, M., Novello, V.F., Stríkis, N.M.,  
469 2019. Coherent South American monsoon variability during the last millennium revealed through  
470 high-resolution proxy records. *Geophys. Res. Lett.* 46, 8261–8270,  
471 <https://doi.org/10.1029/2019GL082513>.

472 Cerling, T.E., 1984. The stable isotopic composition of modern soil carbonate and its relationship to  
473 climate. *Earth. Planet. Sci. Lett.* 71(2), 229-240, [https://doi.org/10.1016/0012-821X\(84\)90089-X](https://doi.org/10.1016/0012-821X(84)90089-X).

474 Cruz, F.W., Burns, S.J., Jercinovic, M., Karmann, I., Sharp, W.D., Vuille, M., 2006. Evidence of rainfall  
475 variations in Southern Brazil from trace element ratios (Mg/Ca and Sr/Ca) in a Late Pleistocene  
476 stalagmite. *Earth Planet Sci. Lett.* 71, 2250-2263, <http://doi:10.1016/j.gca.2007.02.005>.

477 Cruz, F.W., Vuille, M., Burns, S.J., Wang, X., Cheng, H., Werner, M., Edwards, R.L., Karmann, I.,  
478 Auler, A.S., Nguyen, H., 2009. Orbitally driven east-west antiphasing of South American  
479 precipitation. *Nat. Geosc.* 2, 210-214, <http://doi:10.1038/NGEO0444>.

480 Deininger, M., McDermott, F., Mudelsee, M., Werner, M., Frank, N., Mangini, A., 2017. Coherency of  
481 late Holocene European speleothem  $\delta^{18}\text{O}$  records linked to North Atlantic Ocean circulation.  
482 *Climate Dynamics*, 49 (1-2), 595–618, <http://doi.org/10.1007/s00382-016-3360-8>.

483 Dreybrodt, W., 1988. *Processes in Karst Systems. Springer Series in Physical Environment.* Springer,  
484 Heidelberg.

485 Ehleringer, J.R., Cerling, T.E., Helliker, B.R., 1997.  $\text{C}_4$  photosynthesis, atmospheric  $\text{CO}_2$ , and climate.  
486 *Oecologia*, 112, 285-299, <https://doi.org/10.1007/s004420050311>.

487 Fairchild, I.J., Baker, A., 2012 (Eds): *Speleothem Science: From Process to Past Environments*, Wiley-  
488 Blackwell.

489 Fohlmeister, J., Voarintsoa, N.R.G., Lechleitner, F.A., Boyd, M., Brandstätter, S., Jacobson, M.J., Oster,  
490 J., 2020. Main controls on the Stable Carbon Isotope Composition of Speleothems. *Geochim.*  
491 *Cosmochim. Ac.* GCA11710, <https://doi.org/10.1016/j.gca.2020.03.042>.

492 Fohlmeister, J., Scholz, D., Kromer, B., Mangini, A., 2011. Modelling carbon isotopes of carbonates in  
493 cave drip water. *Geochim. et Cosmochim. Ac.* 75(18), 5219-5228,  
494 <https://doi.org/10.1016/j.gca.2011.06.023>.

495 Genty, D., Baker, A., Massault, M., Proctor, C., Gilmour, M., Pons-Branchu, E., Hamelin, B., 2001. Dead  
496 carbon in stalagmites: Carbonate bedrock paleodissolution vs. ageing of soil organic matter.  
497 Implications for  $^{13}\text{C}$  variations in speleothems. *Geochim. Cosmochim. Ac.* 65, 3443-3457,  
498 [https://doi.org/10.1016/S0016-7037\(01\)00697-4](https://doi.org/10.1016/S0016-7037(01)00697-4).

499 Hartman G., Danin A., 2020. Isotopic values of plants in relation to water availability in the Eastern  
500 Mediterranean region. *Oecologia* 162, 837–852, <http://doi.org/10.1007/s00442-009-1514-7>.

501 Hendy, C.H., 1971. The isotopic geochemistry of speleothems 1. The calculation of the effects of the  
502 different modes of formation on the isotopic composition of speleothems and their applicability as  
503 palaeoclimatic indicators. *Geochim. Cosmochim. Ac.*, 35, 801–824, [https://doi.org/10.1016/0016-](https://doi.org/10.1016/0016-7037(71)90127-X)  
504 [7037\(71\)90127-X](https://doi.org/10.1016/0016-7037(71)90127-X).

505 Huffman, G., Bolvin, D.T., Braithwaite, D., Hsu, K., Joyce, R., Xie, P., 2014. Integrated Multi-satellitE  
506 Retrievals for GPM (IMERG), version 4.4. NASA's Precip. Process. Cent.

507 Jaqueto, P., Trindade, R.I.F., Hartmann, G.A., Novello, V.F., Cruz, F.W., Karmann, I., Strauss, B.E.,  
508 Feinberg, J.M., 2017. Linking speleothem and soil magnetism in the Pau d'Alho cave (central South  
509 America). *J. Geophys. Res. Solid. Earth*, 121, <http://doi:10.1002/2016JB013541>.

510 Jia, G., E. Shevliakova, Artaxo P., De Noblet-Ducoudré, N., Houghton, R., House, J., Kitajima, K.,  
511 Lennard, C., Popp, A., Sirin, A., Sukumar, R., Verchot, L., 2019 Land–climate interactions. In:  
512 *Climate Change and Land: an IPCC special report on climate change, desertification, land*  
513 *degradation, sustainable land management, food security, and greenhouse gas fluxes in terrestrial*  
514 *ecosystems* [Shukla, P.R., Skea, J., Calvo Buendia, E., Masson-Delmotte, V., Pörtner, H.-O.,

515 Roberts, D. C., Zhai, P., Slade, R., Connors, S., Van Diemen, Ferrat, R. M., Haughey, E., Luz, S.,  
516 Neogi, S., Pathak, M., Petzold, J., Portugal Pereira, J., Vyas, P., Huntley, E., Kissick, K., Belkacemi,  
517 M., Malley, J. (eds.)]. <https://www.ipcc.ch/srccl/chapter/chapter-2/>.

518 Kanner, L.C., Burns, S.J., Cheng, H., Edwards, R.L., Vuille, M., 2013. High-resolution variability of the  
519 South American summer monsoon over the last seven millennia: insights from a speleothem record  
520 from the central Peruvian Andes. *Quat. Sci. Rev.* 75, 1-10,  
521 <http://doi.org/10.1016/j.quascirev.2013.05.008>.

522 Lachniet, M.S., 2009. Climatic and environmental controls on speleothem oxygen-isotope values. *Quat.*  
523 *Sci. Rev.* 28, 412-432, <https://doi.org/10.1016/j.quascirev.2008.10.021>.

524 Lima, O.N.B., 2011. Estratigrafia isotópica e evolução sedimentar do Grupo Bambuí na borda ocidental  
525 do Cráton do São Francisco: implicação tectônica e paleo-ambiental. Ph.D. thesis, Universidade de  
526 Brasília, Brazil, 114 pp., 2011.

527 McDermott, F., 2004. Palaeo-climate reconstruction from stable isotope variations in speleothems: a  
528 review. *Quat. Sci. Rev.* 23, 901–918, <http://doi.org/10.1016/j.quascirev.2003.06.021>.

529 Meyer, K.W., Feng, W., Breecker, D.O., Banner, J.L., Guilfoyle, A., 2014. Interpretation of speleothem  
530 calcite  $\delta^{13}\text{C}$  variations: Evidence from monitoring soil  $\text{CO}_2$ , drip water, and modern speleothem  
531 calcite in central Texas. *Geochim. Cosmochim. Ac.* 142, 281-298,  
532 <http://doi.org/10.1016/j.gca.2014.07.027>.

533 Mickler, P.J., Carlson, P., Banner, J.L., Breecker, D.O., Stern, L., Guilfoyle, A., 2019. Quantifying  
534 carbon isotope disequilibrium during in-cave evolution of drip water along discrete flow  
535 paths. *Geochim. Cosmochim. Ac.* 244, 182-196, <https://doi.org/10.1016/j.gca.2018.09.027>.

536 Mickler, P.J., Stern, L.A., Banner, J.L., 2006. Large Kinect isotope effects in modern speleothems. *Geol.*  
537 *Soc. Am. Bull.*, 118, 65-81, <http://doi.org/10.1130/B25698.1>.

538 Moquet, J.S., Cruz, F.W., Novello, V.F., Strikis, N.M., Deininger, M., Karmann, I., Santos, R.V., Millo,  
539 C., Apaestegui, J., Guyot, J.-L., Siffedine, A., Vuille, M., Cheng, H., Edwards, R.L., Santini, W.,  
540 2016. Calibration of speleothem  $\text{d}18\text{O}$  records against hydroclimate instrumental records in Central  
541 Brazil. *Global Planet. Change*, 139, 151-164, <https://doi.org/10.1016/j.gloplacha.2016.02.001>.

542 Nogueira, A.C.R., Riccomini, C., 2006. O Grupo Araras (Neoproterozóico) na parte norte da faixa  
543 Paraguai e sul do craton amazônico, Brasil. *Braz. J. Geol.* 36, 576-587.

544 Novello, V.F., Cruz, F.W., Karmann, I., Burns, S.J., Stríkis, N.M., Vuille, M., Cheng, H., Edwards, R.L.,  
545 Santos, R.V., Frigo, E., Barreto, E.A.S., 2012. Multidecadal climate variability in Brazil's Nordeste  
546 during the last 3000 years based on speleothem isotope records. *Geophys. Res. Lett.* 39, L23706,  
547 <http://doi.org/10.1029/2012GL053936>.

548 Novello, V.F., Vuille, M., Cruz, F.W., Stríkis, N.M., Saito de Paula, M., Edwards, R.L., Cheng, H.,  
549 Karmann, I., Jaqueto, P.F., Trindade, R.I.F., Hartmann, G.A., Moquet, J.S., 2016. Centennial-scale  
550 solar forcing of the South American Monsoon System recorded in stalagmites. *Sci. Rep.*, 6, 24762,  
551 <http://doi.org/10.1038/srep24762>.

552 Novello, V.F., Cruz, F.W., Moquet, J.S., Vuille, M., de Paula, M.S.; Nunes, D., Edwards, R.L., Cheng,  
553 H., Karmann, I., Utida, G., Stríkis, N.M., Campos, J.L P.S., 2018. Two millennia of South Atlantic  
554 Convergence Zone variability reconstructed from isotopic proxies. *Geophys. Res. Lett.* 45,  
555 <http://doi.org/10.1029/2017GL076838>.

556 Novello, V.F., Cruz, F.W., McGlue, M.M., Wong, C.I., Ward, B.M., Vuille, M., Santos, R.A., Jaqueto, P.,  
557 Pessenda, L.C.R., Atorre, T., Ribeiro, L.M.A.L., Karmann, I., Barreto, E.S., Cheng, H., Edwards, R.  
558 L., Paula, M.S., Scholz, D., 2019. Vegetation and environmental changes in tropical South America  
559 from the last glacial to the Holocene documented by multiple cave sediment proxies. *Earth Planet.*  
560 *Sci. Lett.* 524, 115717, [doi.org/10.1016/j.epsl.2019.115717](https://doi.org/10.1016/j.epsl.2019.115717).

561 Ohmura, A., 2012. Enhanced temperature variability in high-altitude climate change. *Theor. Appl.*  
562 *Climatol.* 110, 499-508, <https://doi.org/10.1007/s00704-012-0687-x>.

563 Olson, D.M., Dinerstein, E., Wikramanayake, E.D., Burgess, N.D., Powell, G.V.N., Underwood, E.C.,  
564 D'amico, J.A., Itoua, I., Strand, H.E., Morrison, J.C., Loucks, C.J., Allnut, T.F., Ricketts, T.H., Kura,  
565 Y., Lamoreus, J.F., Wettengel, W.W., Hedao, P., Kassem, K.R., 2001. Terrestrial Ecoregions of the  
566 World: A New Map of Life on Earth. *Bioscience*, 51, 933-938, [http://doi.org/10.1641/0006-](http://doi.org/10.1641/0006-3568(2001)051[0933:TEOTWA]2.0.CO;2)  
567 [3568\(2001\)051\[0933:TEOTWA\]2.0.CO;2](http://doi.org/10.1641/0006-3568(2001)051[0933:TEOTWA]2.0.CO;2).

568 Pansani, T.R., Muniz, F.P., Cherkinsky, A., Pacheco, M.L.A. F., Dantas, M.A.T., 2019. Isotopic  
569 paleoecology ( $\delta^{13}\text{C}$ ,  $\delta^{18}\text{O}$ ) of Late Quaternary megafauna from Mato Grosso do Sul and Bahia States,  
570 Brazil. *Quat. Sci. Rev.*, 221, 105864, <https://doi.org/10.1016/j.quascirev.2019.105864>.

571 Pessenda, L.C.R., Gouveia, S.E.M., Ribeiro, A.S., Oliveira, P.E., Aravena, R., 2020. Late Pleistocene and  
572 Holocene vegetation changes in northeastern Brazil determined from carbon isotopes and charcoal  
573 records in soil. *Palaeogeogr. Palaeocl.* 297, 597-608, <http://doi.org/10.1016/j.palaeo.2010.09.008>.

574 Polag, D., Scholz, D., Mühlinghaus, C., Spötl, C., Schröder-Ritzrau, A., Segl, M., Mangini, A., 2010.  
575 Stable isotope fractionation in speleothems: Laboratory experiments. *Chem. Geol.* 279, 31-39,  
576 <https://doi.org/10.1016/j.chemgeo.2010.09.016>.

577 Quade, J., Cerling, T.E., Bowman, J.R., 1989. Systematic variations in the carbon and oxygen isotopic  
578 composition of pedogenic carbonate along transects in the Southern Great Basin, United States. *Geol.*  
579 *Soc. Am. Bull.*, 101: 464-475, [https://doi.org/10.1130/0016-](https://doi.org/10.1130/0016-7606(1989)101<0464:SVITCA>2.3.CO;2)  
580 [7606\(1989\)101<0464:SVITCA>2.3.CO;2](https://doi.org/10.1130/0016-7606(1989)101<0464:SVITCA>2.3.CO;2).

581 Rayner, P.J., Enting, I.G., Francey, R.J., Langenfelds, R., 1999. Reconstructing the recent carbon cycle  
582 from atmospheric  $\text{CO}_2$ ,  $\delta^{13}\text{C}$  and  $\text{O}_2/\text{N}_2$  observations. *Tellus B*, 51:2, 213-232,  
583 <http://doi.org/10.3402/tellusb.v51i2.16273>.

584 Reuter, J., Stott, L., Khider, D., Sinha, A., Cheng, H., Edwards, R.L., 2009. A new perspective on the  
585 hydroclimate variability in northern South America during the Little Ice Age. *Geophys. Res. Lett.* 36,  
586 L21706, <http://doi.org/10.1029/2009GL041051>.

587 Salomons, W., Mook, W.G., 1986. Isotope geochemistry of carbonates in the weathering zone. In: Fritz,  
588 P., Fontes, C.J. (Eds.), *Handbook of Environmental Isotope Geochemistry*, Vol. 2. The Terrestrial  
589 Environment, B. Elsevier, Amsterdam.

590 Schubert, B.A., Jahren, A.H., 2012. The effect of atmospheric  $\text{CO}_2$  concentration on carbon isotope  
591 fractionation in  $\text{C}_3$  land plants. *Geochim. Cosmochim. Ac.*, 96, 29-43,  
592 <https://doi.org/10.1016/j.gca.2012.08.003>.

593 Strikís, N. M., 2015. Atividade do Sistema de Monção Sul-americana na porção central do Brasil durante  
594 o último período glacial a partir da aplicação de isótopos de oxigênio em espeleotemas, Ph.D. thesis,  
595 Instituto de Geociências, Universidade de São Paulo, Brazil, 265 pp..

596 Utida, G., Cruz, F.W., Santos, R.V., Sawakuchi, A.O., Wang, H., Pessenda, L.C.R., Novello, V.F., Vuille,  
597 M., Stríkis, N.M., Guedes, C., Cheng, H., Edwards, R.L., 2020. Climate changes in Northeastern  
598 Brazil from Deglacial to Meghalayan periods and related environmental impacts. *Quat. Sci. Rev.*,  
599 250, 106655, <https://doi.org/10.1016/j.quascirev.2020.106655>.

600 Van de Water, P. K., Leavitt, S. W. and Betancourt, J. L.: Trends in stomatal density and  $^{13}\text{C}/^{12}\text{C}$  ratios  
601 of *Pinus flexilis* needles during last glacial-interglacial cycle. *Science*, 264(5156), 239-243, 1994.

602 Vuille, M., Burns, S.J., Taylor, B.L., Cruz, F.W., Bird, B.W., Abbott, M.B., Kanner, L. C., Cheng, H.,  
603 Novello, V.F., 2012. A review of the South American Monsoon history as recorded in stable isotopic  
604 proxies over the past two millennia. *Clim. Past*, 8(4), 1309–1321, [http://doi.org/10.5194/cp-8-1309-](http://doi.org/10.5194/cp-8-1309-2012)  
605 2012.

606 Wang, X., Edwards, R.L., Auler, A.S., Cheng, H., Kong, X., Wang, Y., Cruz, F.W., Dorale, J.A.D.,  
607 Chiang, H.-W., 2017. Hydroclimate changes across the Amazon lowlands over the past 45,000 years.  
608 *Nature*, 541, 204 – 209, <http://doi.org/10.1038/nature20787>.

609 Wortham, B.E., Wong, C.I., Silva, L.C.R., McGee, D., Montañez, I.P., Rasbury, E.T., Cooper, K.M.,  
610 Sharp, W.D., Glessner, J.J.G., Santos, R.V., 2017. Assessing response of local moisture conditions in  
611 central Brazil to variability in regional monsoon intensity using speleothem  $^{87}\text{Sr}/^{86}\text{Sr}$  values. *Earth*.  
612 *Planet. Sci. Lett.* 463, 310-322, <http://doi.org/10.1016/j.epsl.2017.01.034>.

613

614 **Author contribution:** VFN designed the experiments, FWC and MV are the project PIs, JLPSC  
615 performed statistical analysis, NMS and JSM performed isotopic analyses, VA, GU, PJ, IK, LCRP and  
616 DOB assisted in the discussion and interpretations. AA created the map, GMPS provided a review on  
617 carbonate formations. VFN prepared the manuscript with contributions from all co-authors.

618

#### 619 **Acknowledgements**

620 We thank the São Paulo Research Foundation (FAPESP) for financial support through grants  
621 2016/15807-5 to VFN, 2017/50085-3, and 2019/07794-9 to FWC and the US National Science  
622 Foundation for award OISE-1743738 to MV. We thank the Instituto Chico Mendes de Conservação da

623 Biodiversidade (ICMbio) for providing the permission (number 22424-8) to undertake the cave studies in  
624 Brazil.